Superconducting Quantum Interference Device (SQUID) Magnetometers

Matthias Schmelz and Ronny Stolz

Abstract Direct Current Superconducting QUantum Interference Devices (dc SQUIDs) are sensors for the detection of magnetic flux or any physical quantity that can be transformed into magnetic flux. They consist of a superconducting loop interrupted by two resistively shunted Josephson tunnel junctions. Typically operated at 4.2 K, they exhibit magnetic flux noise levels of the order of 1 $\mu\Phi_0/\mathrm{Hz}^{1/2}$, corresponding to a noise energy of 10^{-32} $\mathrm{J/Hz}^{1/2}$. They can be used for example as magnetometers, magnetic gradiometers, current sensors and voltmeters, susceptometers or (rf) amplifier. With their large bandwidth and flat frequency response ranging from dc to GHz, they are excellent suited for a wide variety of applications, such as e.g. biomagnetism and geophysical exploration to the detection of gravity waves and magnetic resonance.

1 Introduction

SQUIDs are today's most sensitive devices for the detection of magnetic flux Φ. They convert magnetic flux or any physical property that can be transformed into magnetic flux, for example magnetic flux density B, into e.g. a voltage across the device. The operation of SQUIDs is based on two physical phenomena: flux quantization in a closed superconducting loop in units of the flux quantum $\Phi_0 = h/2e = 2.07 \times 10^{-15}$ Tm^2, and Josephson tunneling.

Superconductivity represents a thermodynamic state—existing below a critical temperature T_C—in which e.g. current is carried by pairs of electrons with opposite momentum and spin, so-called Cooper pairs. For metallic low-temperature superconductors (LTS), like the most widely used Nb, T_C is usually below 10 K. Low

M. Schmelz (✉) · R. Stolz
Leibniz Institute of Photonic Technology, Albert-Einstein-Straße 9,
07745 Jena, Germany
e-mail: matthias.schmelz@ipht-jena.de

R. Stolz
e-mail: ronny.stolz@ipht-jena.de

A. Grosz et al. (eds.), *High Sensitivity Magnetometers*, Smart Sensors,
Measurement and Instrumentation 19, DOI 10.1007/978-3-319-34070-8_10

operation temperatures permit very sensitive measurements but require the use of cryogenics. Although high-temperature superconductors (HTS) have relaxed demands on the cooling system, we will restrict this overview to LTS devices due to their lower intrinsic noise, higher reliability and the potential for an industrial-like fabrication process. The general considerations remain the same for HTS devices. Among the variety of SQUID types, we will focus on dc SQUIDs, since they typically feature superior noise performance compared with rf SQUIDs and are therefore of main significance nowadays.

In this chapter we will give an overview on SQUIDs, their operation principle and design guidelines. We will describe fabrication techniques and comment on associated SQUID electronics. Due to the limited space available, the emphasis is on the understanding of such sensors in view of their practical applicability. For an in-depth view on superconductivity and on its various effects, we refer to the excellent textbooks available [1, 2]. Moreover, a number of books deal in much greater detail with various research topics we can just briefly touch, and offer a detailed view on theory as well as on the application of these devices [3–6].

In Sect. 2 we will briefly review Josephson tunnel junctions as the most important part of SQUIDs and describe basic effects and relations. In Sect. 3 we will delineate how these devices are fabricated and operated. We comment on their sensitivity limitations and how different types of SQUIDs are tailored to the envisaged application. Section 4 review results achieved with state-of-the-art devices aimed for a number of the mentioned applications, and in Sect. 5 we provide some concluding remarks and an outlook.

2 SQUID Fundamentals

The dc SQUID, as first proposed by Jaklevic et al. in 1964 [7], consists of a superconducting loop with inductance L_{SQ} interrupted by two Josephson junctions. Before discussing the operation principle of SQUIDs, we will briefly review Josephson tunnel junctions and related basic effects.

2.1 Josephson Junctions

As described earlier, the current in a superconductor is carried by so-called Cooper pairs. Since these pairs have zero spin, they follow boson statistics. As a consequence, they all condense in the same quantum state and can be described by a collective superconducting wave function $\Psi = \Psi_0 \cdot \exp(i\phi)$, with $\phi(x,t)$ being the time and space dependent phase and $n_S = |\Psi|^2$ the Cooper pair density.

If two superconductors are weakly connected, Cooper pairs can exchange between them. There are different types of how these weak links or junctions can be arranged. Probably the most important type and the one we will focus on is the

so-called SIS Josephson tunnel junction, where a thin insulating barrier (I) is placed between two superconductors (S). The current through the Josephson junction is described by the first Josephson equation $I_C = I_{C,0} \sin(\varphi)$, with $\varphi = \phi_1 - \phi_2$ being the phase difference across the junction [8]. Here $I_{C,0}$ is the junction's maximum critical current which is determined by the thickness of the insulating barrier t_{ox}, the junction area A_{JJ} and the operation temperature T.

When the maximum critical current is exceeded, the phase difference across the junction will evolve over time and a dc voltage across the junction appears. It is described by the second Josephson equation [8]

$$\frac{\partial \varphi}{\partial t} = \frac{2\mathrm{e}}{\hbar} \cdot V_{DC} = \frac{2\pi}{\Phi_0} \cdot V_{DC}, \tag{1}$$

where $\hbar = 1.055 \times 10^{-34}$ Js is the reduced Planck's constant. Please note that subsequently V represents the time averaged dc voltage over the junction. In fact the Josephson current oscillates with the Josephson frequency $2\pi V_{DC}/\Phi_0$, when biased with $I > I_{C,0}$.

A typical current-voltage characteristic of an undamped Josephson junction exhibits a hysteresis, as shown in Fig. 1 (left). A measure for this hysteresis is the McCumber parameter [9, 10]

$$\beta_C = \frac{2\pi I_C R^2 C_{JJ}}{\Phi_0}. \tag{2}$$

In order to avoid the hysteresis and therefore to obtain a single valued characteristic depicted in the right panel of Fig. 1, an additional shunt resistor R_S is usually placed across the junction to damp its dynamics, which is fulfilled for the condition $\beta_C < 1$. The dynamics of Josephson junctions are typically described in the

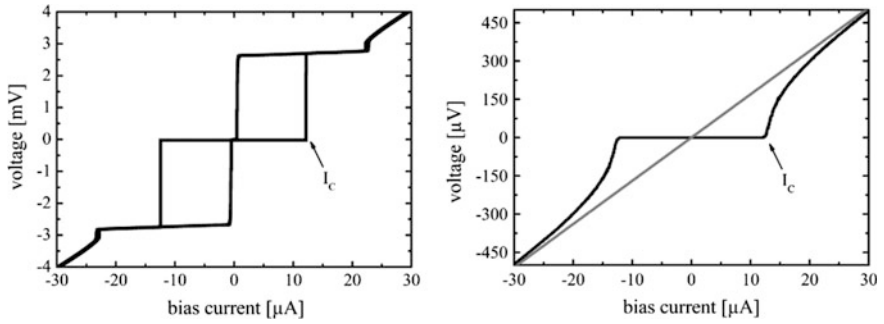

Fig. 1 (*Left*) Current-voltage characteristics of an undamped and (*Right*) of a damped (shunted) Josephson tunnel junction. The critical current of the junction I_C is about 10 μA, as indicated. For large bias currents, the characteristic of the shunted junction converges into an ohmic behavior, given by the shunt resistor value

so-called RCSJ (resistively and capacitively shunted junction) model. Therein a real Josephson junction is composed of an ideal one with additional resistance R and capacitance C_{JJ} in parallel, describing the tunneling of normal electrons in the voltage state and the displacement current over the capacitance between the two superconducting electrodes, respectively.

Due to finite thermal energy at temperatures $T > 0$, the I-V characteristic of a non-hysteretic junction is noise-rounded for currents of about I_C, as can be seen in Fig. 1 (right). The ratio between thermal energy $k_B T$ and Josephson coupling energy $E_J = I_C \Phi_0 / 2\pi$ describes the strength of noise-rounding due to thermal noise of the shunt resistor [11, 12] and is known as the noise parameter

$$\Gamma = \frac{k_B T}{E_J} = \frac{2\pi k_B T}{I_C \Phi_0} \tag{3}$$

Here, k_B is Boltzmann's constant. In LTS dc SQUIDs the influence due to thermal noise-rounding is typically neglected for $\Gamma < 0.05$.

2.2 dc SQUIDs

2.2.1 Operation Principle

As Cooper pairs can be described by a single valued wave function, the phase difference $\Delta\phi$ along an arbitrary closed path $\vec{l}$ inside a superconductor has to be a multiple of 2π. Accordingly, the magnetic flux Φ inside a superconductor can only take integer values of the magnetic flux quantum Φ_0. The externally applied flux Φ_{ext} to a superconducting loop is therefore compensated in units of Φ_0 by an appropriate self-induced flux $\Phi = L_{SQ} \cdot I_{Circ}$ due to a circulating shielding current I_{Circ} in the loop.

For the subsequent discussion, let us assume two identical junctions, each with critical current I_C, which are arranged symmetrically in the SQUID loop, as illustrated in Fig. 2. If the SQUID is biased with a constant current $I_B \geq 2I_C$, the bias current is equally divided between the two branches. As an external flux Φ_{ext} leads to a circulating current to fulfil the flux quantization in the loop, the bias current in a SQUID is redistributed in dependence of the external magnetic flux. For $\Phi_{ext} = n\Phi_0$ no circulating screening current flows and the critical current of the SQUID is just $I = 2I_C$, whereas $\Phi_{ext} \neq n\Phi_0$ leads to a suppression of the critical current of the SQUID. The critical current of a SQUID—or in case of a constant current bias the voltage across the SQUID—hence modulates between the two extremal values $\Phi_{ext} = n\Phi_0$ and $\Phi_{ext} = n\Phi_0/2$ and has a periodic dependence on Φ_{ext} as shown in Fig. 3. A measure for the suppression of the critical current of the SQUID is the dimensionless screening parameter

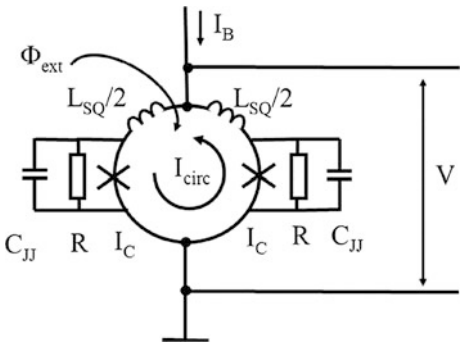

Fig. 2 Schematic of a dc SQUID with two Josephson junctions with SQUID inductance L_{SQ}, critical currents I_C, junction capacitance C_{JJ}, and resistance R. The external flux Φ_{ext}, coupled to the SQUID loop, results in a circulating screening current I_{circ}, which modulates the measured voltage V across the SQUID

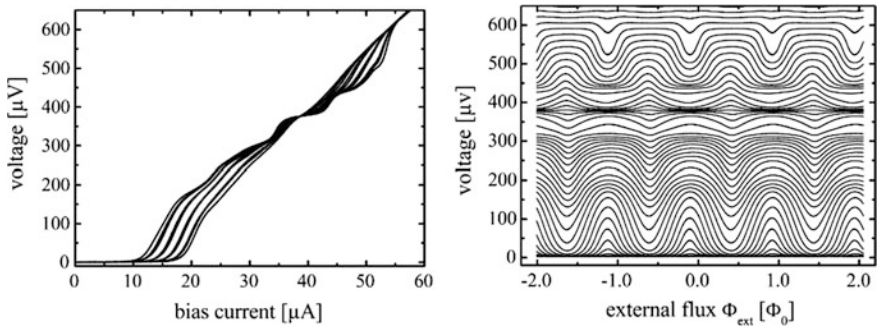

Fig. 3 (*Left*) Measured *I-V* characteristics of a SQUID for Φ_{ext} ranging between $\Phi_{ext} = n\Phi_0$ and $\Phi_{ext} = (2n + 1)\Phi_0/2$ and (*Right*) corresponding set of flux-voltage characteristics for bias currents from 0 μA to 55 μA in steps of 1μA. The flux-voltage characteristics represent the projection of the current-voltage characteristics for modulating external flux Φ_{ext}. The kinks in the current-voltage characteristics are due to resonances occurring in the SQUID, as will be discussed later

$$\beta_L = \frac{2L_{SQ}I_C}{\Phi_0}. \tag{4}$$

For $\beta_L \ll 1$ the current swing ΔI approaches $2I_C$, whereas for $\beta_L \gg 1$ it reduces to zero.

The SQUID may be operated with constant current (so-called current bias) or constant voltage (voltage bias). In current bias mode it is typically operated on the steep part of the flux-voltage characteristics, where the transfer coefficient $V_\Phi = \partial V/\partial\Phi$ is maximum. In the small signal limit ($\Phi_{ext} \ll \Phi_0$) it therefore converts an external magnetic flux Φ_{ext}, or other physical quantities that can be transformed into

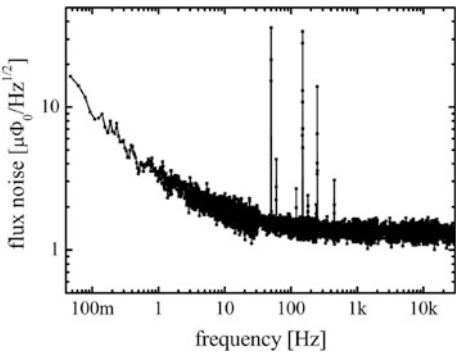

Fig. 4 Typical flux noise spectrum of a dc SQUID measured at 4.2 K. The SQUID has an inductance of L_{SQ} = 180 pH and a normal resistance of $R \approx 10\ \Omega$. The equivalent white flux noise accounts to 1.3 $\mu\Phi_0/\mathrm{Hz}^{1/2}$

magnetic flux, into a voltage across the SQUID. Since the external flux typically exceeds the small signal limit, the SQUID is usually operated in a so-called flux-locked-loop (FLL) feedback circuit, which will be discussed in the subsequent Sect. 2.3.

2.2.2 Noise in dc SQUIDs—White and 1/f Noise

The noise in SQUIDs has two contributions: a frequency independent white and a colored noise, which increases at low frequencies. The colored part of the spectrum is called 1/f noise, too. A representative spectrum of flux noise[1] is shown in Fig. 4. At 4.2 K typically Nyquist noise of the shunt resistors is the dominant source of white noise. It has been shown [13] that for optimum conditions ($\beta_C = \beta_L \approx 1$) the power spectral density of voltage noise is given by

$$S_V(f) \approx 16 k_B T R, \tag{5}$$

which is equivalent to a flux noise with spectral density

$$S_\Phi(f) = S_V / V_\Phi^2 = 16 k_B T L_{SQ}^2 / R. \tag{6}$$

Here, the approximation $V_\Phi = R/L_{SQ}$ for the transfer coefficient is used. Please note, that the measured noise is roughly four times the Nyquist noise due to mixing down effects in the SQUID.

In order to compare SQUIDs with different inductances L_{SQ}, one usually refers to the equivalent energy resolution $\varepsilon = S_\Phi / 2L_{SQ}$—the energy of the signal equal to the intrinsic noise energy in the unit bandwidth. For the optimum conditions above

[1]The equivalent flux noise $S_\Phi^{1/2}$ is given by the measured voltage noise $S_V^{1/2}$ and the transfer function V_Φ as $S_\Phi^{1/2} = S_V^{1/2} / V_\Phi$.

one can rewrite these relations as a function of the SQUID inductance L_{SQ} and junction capacitance C_{JJ} as

$$\sqrt{S_\Phi(f)} = 4 \cdot L_{SQ}^{3/4} C_{JJ}^{1/4} \cdot \sqrt{2k_B T} \text{ and} \tag{7}$$

$$\varepsilon(f) = 16 k_B T \sqrt{L_{SQ} C_{JJ}}. \tag{8}$$

where we have set $\beta_C = \beta_L = 1$.

Typically, the white flux noise of LTS dc SQUIDs operated at 4.2 K is of the order of 10^{-6} $\Phi_0/\text{Hz}^{1/2}$ and the energy resolution amounts to 10^{-32} $\text{J/Hz}^{1/2}$, corresponding to several h, with h being Planck's constant. For temperatures of about 0.3 K a noise energy of about 2 ħ has been achieved for SQUIDs with $L_{SQ} \approx 100$ pH [14]. For such a SQUID inductance the condition $\beta_L = 1$ results in a junction's critical current of about $I_C \approx 10$ μA, which is a typical value for low noise SQUIDs.

It is obvious from the relation above that the energy resolution can be improved by reducing the SQUID inductance, the working temperature and the junction capacitance.

However, for practically applicable sensors the coupling to an external signal imposes a lower limit for the SQUID inductance. The effective flux capture area of e.g. a square washer SQUID scales with the linear dimension of the washer hole, which in turn is proportional to L_{SQ}. Hence, there is a tradeoff between a small inductance for a high energy resolution and a large inductance for a sufficiently effective area and therefore for adequate coupling to external signals

The working temperature of LTS dc SQUIDs is typically fixed—either at 4.2 K or even lower temperatures, determined by the measurement task and available cooling devices. To further enhance the SQUID performance in terms of noise, the total junction capacitance C_{JJ} and hence the junction size needs to be reduced, which is typically limited by the used fabrication process. Furthermore, small area junctions can take advantage of their low capacitance only if careful attention is also been paid on the immediate surroundings of the junctions. An undesired parasitic capacitance $C_{JJ,p}$ due to a nearby overlap of superconducting electrodes may affect or even dominate the performance of superconducting devices. This requirement will be discussed in more detail in Sect. 3.

In addition to the white noise discussed above, below a certain frequency f_C, known as the 1/f corner, the noise increases with $1/f^\alpha$, where α ranges between 0.5 and 1.0. At f_C the contribution of white noise equals the contribution of 1/f noise and may be below 1 Hz. Several sources of low-frequency noise in dc SQUIDs have been identified so far. According to [15] one can distinguish between fluctuations in critical currents of the Josephson junctions and flux noise.

It is generally accepted that critical current fluctuations originate in a random trapping and release of electrons in defect states in the junction barrier. Therefore the barrier height and in this way the critical current of the Josephson junction is locally changed, which leads to a random telegraph noise. The superposition of

many of these fluctuations, each with its own characteristic lifetime, leads to a $1/f$ dependence of the power spectral density of the flux noise S_Φ [16]. As we will see in Sect. 2.3, the influence of critical current fluctuations can be reduced or even eliminated by use of an adequate electronic readout scheme.

The second source of noise, so-called flux noise, arises from the movement of trapped vortices—small non-superconducting regions inside the superconductor—in the SQUID washer. The affinity to trap flux in superconducting structures can be expressed by calculating Gibbs free energy [17–19]. According to these estimations, a small linewidth of the superconductor is usually favorable to prevent vortex trapping in the superconductor during cool-down in an ambient magnetic field. By reducing the linewidth w of superconducting structures to below $w \approx (\Phi_0/B)^{1/2}$ this kind of flux noise can in principle be eliminated. For a magnetic flux density $B \approx 50$ μT this results in $w < 6$ μm.

More recently another source of low-frequency flux noise has been identified, but up to now there is no comprehensive understanding of this phenomenon. During the last years several possible candidates to explain the microscopic origin of this low-frequency flux noise have been discussed. For example Koch et al. [20] suggested that spins of unpaired electrons on the surface of the superconductor, hopping on and off defect states due to thermal activation, may produce such a signature. In this case, the direction of the spins would be locked as long as the electrons are trapped, thus contributing a random magnetic signal. The superposition of many uncorrelated changes of spin direction would thereafter sum up to the observed $1/f$ power spectrum.

As the power spectral density of flux noise scales with V_Φ, this contribution vanishes in working points with $\partial V/\partial \Phi = 0$, whereas critical current fluctuations do not. This allows for an independent estimation and optimization for the contributions of critical current and magnetic flux noise. Although the question about the origin of this kind of flux-noise is still an unsolved puzzle, it seems that the quality of the superconducting film and its interface to e.g. the substrate play an important role for the amount of this $1/f$ flux noise and one may expect considerable improvements in the future.

2.2.3 Practical Devices

As already discussed, a dc SQUID consists of a superconducting loop with inductance L_{SQ} interrupted by two Josephson junctions. Nowadays SQUIDs are typically fabricated in thin film technology, rather than the bulk material SQUIDs that were used in the beginning. In Sect. 3 we will discuss the main steps for the fabrication of modern highly sensitive devices.

Let us now consider one of the simplest designs: the square washer SQUID. Therein the SQUID inductance is shaped as a washer with inner and outer dimensions d and D, as shown in Fig. 5 (left).

Although these “bare” or uncoupled SQUIDs, as no external signal other than the flux threading the hole is coupled to the SQUID, have small inductances given

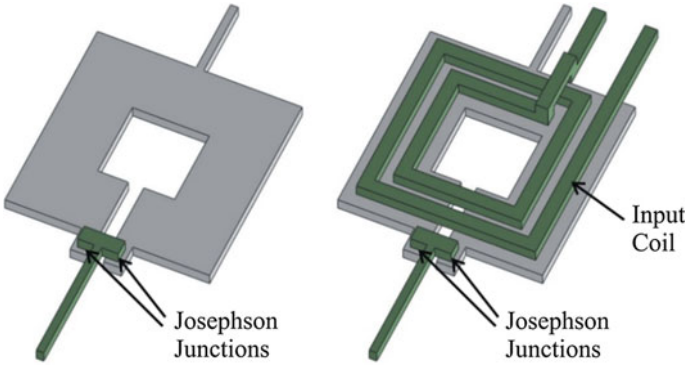

Fig. 5 (*Left*) Model of an uncoupled and (*Right*) of a coupled square washer SQUID. The SQUID inductance is shaped as a square washer with a hole in the center and a slit. The Josephson junctions are located at the outer edge of the slit, as indicated. The coupled SQUID exhibits an input coil on top of the SQUID washer

by $L_{SQ} \approx \mu_0 d$, they exhibit a very small effective flux capture area of about $A_{eff} = \partial\Phi/\partial B = dD$ [21] and therefore poor magnetic field noise

$$\sqrt{S_B(f)} = \sqrt{S_\Phi(f)}/A_{eff}. \tag{9}$$

They are favorable for applications where a good spatial resolution is needed, like in SQUID microscopy or miniature susceptometers [22].

To increase the effective area of these devices without changing their inductance one can simply increase the outer dimension D of the washer, and make use of the flux-focusing effect due to perfect diamagnetism in superconductors. Although this method has successfully been applied especially in high-temperature superconductor devices, the increased linewidth w of the superconductor may deteriorate the low-frequency performance due to trapped flux.

A more effective approach is to place a multi-turn thin film input coil on top of the SQUID washer to ensure a tight inductive coupling between both, as illustrated in Fig. 5 (right). These two layers are separated from each other by an insulating layer. Now a separate pickup loop with much larger effective area can be connected to this input coil to improve the magnetic field resolution. In addition to the input coil, a second coil is typically integrated on top of the SQUID washer in order to couple a feedback signal to the SQUID, as will be discussed in Sect. 2.3.

By integrating a thin-film input coil, SQUIDs can be implemented not only as SQUID magnetometer, but also as sensors for any physical quantity that can be transformed into magnetic flux. Magnetic gradiometers, current sensors and voltmeters, susceptometers, (rf) amplifier or displacement sensors are possible implementations. SQUIDs are therefore very versatile and their applications range from biomagnetism [23, 24] and geophysical exploration [25, 26] to magnetic resonance imaging [27]. Typical sensitivities of SQUIDs for some of these application

Table 1 Typical sensitivities of SQUID sensors

Measurement	Sensitivity
Magnetic field	10^{-15} T/Hz$^{1/2}$
Current	10^{-13} A/Hz$^{1/2}$
Voltage	10^{-14} V/Hz$^{1/2}$
Resistance	10^{-12} Ω
Magnetic moment	10^{-10} emu

scenarios are listed in Table 1. In Sect. 4 we will provide more information on some state-of-the art devices.

As discussed in Sect. 2.2, for the comparison of SQUIDs with different inductances L_{SQ}, one usually refers to the equivalent energy resolution ε. As this describes the energy resolution of an uncoupled SQUID, in practice the so-called coupled energy resolution ε_C is used, which is given by

$$\varepsilon_c = \varepsilon / k_{in}^2 \tag{10}$$

with k_{in} being the coupling constant between the input coil inductance L_{in} and the SQUID loop inductance L_{SQ}. It is determined via the mutual inductance M_{in} between the input coil and the SQUID

$$M_{in} = k_{in} \sqrt{L_{SQ} L_{in}}. \tag{11}$$

According to the definition of ε, the coupled energy resolution ε_C corresponds to the minimum energy that can be detected in the input coil per unit bandwidth. Depending on the intended application and accordingly L_{in}, present SQUIDs exhibit coupled energy resolutions of below 100 h.

The design of coupled SQUIDs on the base of washer SQUIDs is rather straightforward and can easily be carried out based on experimentally proven expressions [28, 29]: The SQUID inductance is thus given by

$$L_{SQ} = L_h + L_s + L_j \tag{12}$$

Here L_h is the inductance of the washer hole, L_s the inductance of the slit and L_j the inductance associated with the Josephson junctions (which typically can be neglected). The inductance of the washer hole is

$$L_h = \alpha \mu_0 d \tag{13}$$

with $\alpha = 1.25$ for square washer, $\alpha = 1.05$ for an octagonal washer and $\alpha = 1$ for a circular washer. The slit inductance can be approximated by

$$L_s = 0.3\,\mathrm{pH}/\mu\mathrm{m}. \tag{14}$$

The mutual inductance between the SQUID and an integrated multi-turn input coil on top of the SQUID washer is given by

$$M_{in} \approx nL_{SQ}. \tag{15}$$

The inductance of the input coil can be expressed as

$$L_{in} \approx n^2 L_{SQ}. \tag{16}$$

The input coil inductance should be matched to the inductance of the pickup circuit for optimum coupling. In case of a SQUID magnetometer the pickup loop is typically a thin film or wire wound loop with inductance L_p, as shown in Fig. 6.

The shape of the pickup circuit has to be adapted to the measurement task, as shown for planar and axial first order gradiometers in Fig. 6.

In practical devices, however, deviations from the ideal behavior may appear, as e.g. stray capacitances between the SQUID washer and the input coil can lead to resonances in the flux-voltage characteristics and may therefore strongly deteriorate the device performance. In consequence, a careful design optimization procedure is typically required for such tightly coupled SQUIDs. Detailed information on this topic can be found e.g. in [30, 31].

Although the coupled energy resolution is a good method to compare SQUIDs with different inductances, the figure of merit for e.g. a magnetometer is the magnetic field noise $S_B^{1/2}$. It has been shown that the magnetic field resolution and hence the magnetic field noise $S_B^{1/2}$ can be improved by increasing the pickup loop area while maintaining $L_{in} \approx L_p$. In Ref. [32] the approximation for the white noise level of $S_B^{1/2}$ vs. the radius r_p of the pickup loop is given as

$$\sqrt{S_B} \approx \frac{2\sqrt{\mu_0 \epsilon}}{r_p^{3/2}}. \tag{17}$$

For a circular pickup loop area with $r_p = 15$ mm and $\varepsilon = 10^{-32}$ Js this results in $S_B^{1/2} \approx 100 \times 10^{-16}$ T/Hz$^{1/2}$ = 0.1 fT/Hz$^{1/2}$.

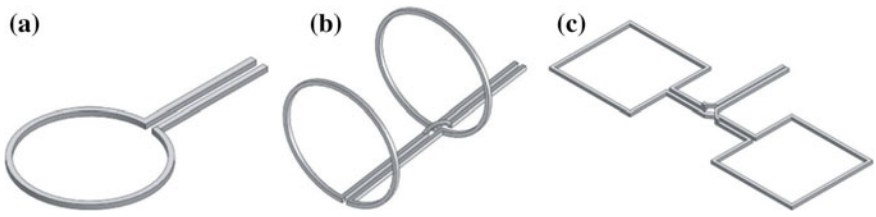

Fig. 6 Common pickup loop configurations: **a** represents a magnetometer, **b** a first order axial gradiometer and **c** a first order planar gradiometer. The two ends of the pickup loops are connected to an integrated input coil on top of the SQUID washer

It is worth to note at this point that although the SQUID sensor by itself may exhibit such an excellent noise performance, the overall noise performance of the SQUID system may be impaired by e.g. noise of the readout circuit as well as the environment as for example by noise arising from the dewar.

Another way to increase the effective area of the magnetometer while maintaining the SQUID inductance at a tolerable level is to divide the superconducting pickup loop into a number of separate loops connected in parallel in order to reduce the total SQUID inductance. In these so-called multiloop magnetometers, as described in detail in [33–36], the SQUID itself typically acts as the sensitive area, whereas the so-called Ketchen-type SQUID is inductively coupled to an antenna as discussed above. Due to inevitable losses owing to the used flux transformer in inductively coupled SQUIDs, the multiloop magnetometer allows for the best field resolution for a given chip area, as for instance described for first order gradiometers in [37].

However, transformer-coupled SQUIDs offer the possibility to include thin-film low-pass filters in the design to increase their robustness—especially for electromagnetically unshielded operation. As an example, Fig. 7 depicts the inner part of a transformer-coupled SQUID with the Josephson junctions [38]. The SQUID itself is shaped in form of a clover leaf with the input coil on top. The layout of the SQUID as a first order gradiometer results in its insensitivity to homogenous ambient field and it may thus be operated as a current sensor.

2.3 SQUID Electronics

As introduced above, the SQUID itself acts as a very sensitive magnetic flux-to-voltage transducer with nonlinear periodic flux-to-voltage characteristic (Fig. 3). In order to obtain a linear dependence of the voltage across the SQUID

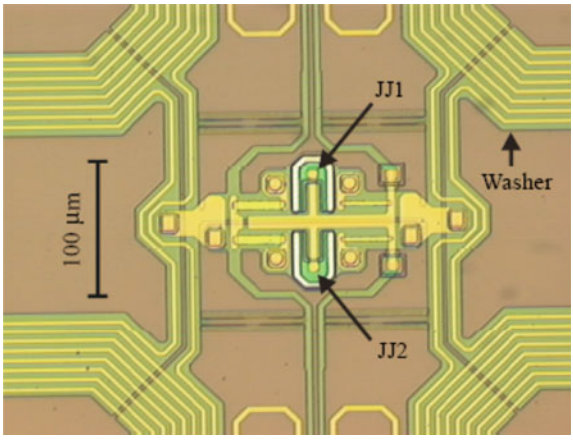

Fig. 7 Microphotograph of the central part of a transformer-coupled SQUID current sensor with the two Josephson junctions indicated as JJ1 and JJ2. The *yellow lines* on top of the SQUID washers represent the input coil. Reprinted from Reference [38], reproduced with permission of IOP Publishing Ltd

from the flux threading the SQUID loop, the SQUID is operated in a feedback loop called flux-locked loop (FLL).

2.3.1 Flux Locked Loop

There are two main FLL schemes [39]: flux-modulation and directly coupled readout.

Due to its ability for the design of compact readout circuits, which are suitable for the use in multi-channel systems with a sufficiently large bandwidth and dynamic range as well as lower power consumption, the directly coupled SQUID electronics is typically used nowadays. We will therefore restrict the discussion to this type of FLL, although the basic concept holds for both.

Before going into details of the directly coupled readout, it should be mentioned that with the flux-modulation readout scheme the preamplifier low-frequency noise and in-phase critical current fluctuations of the Josephson junctions are suppressed. As critical current fluctuations in state-of-the-art LTS tunnel junctions are generally very weak, this is not a major concern for most applications. There are as well readout options like bias reversal [15, 40], which allow suppressing in-phase and out-of-phase critical current fluctuations in both readout schemes.

The directly coupled readout scheme is schematically shown in Fig. 8. The voltage across the SQUID due to a changing signal flux Φ_{Sig} is amplified, integrated and fed back to the SQUID as a feedback flux Φ_{Fb} via a feedback resistor R_{Fb} and a mutual inductance M_{Fb}.

The FLL therefore keeps the flux inside the SQUID constant and the output voltage, the voltage across the feedback resistor, becomes linearly dependent on the applied signal Φ_{Sig} with a strongly increased linear working range.

Besides the linearization, the main purpose of the electronics is to read out the voltage across the SQUID without compromising the low voltage noise level of the SQUID. The influence of the read-out electronics on the total measured flux noise $S_{\Phi,t}^{1/2}$ can be expressed as [39]

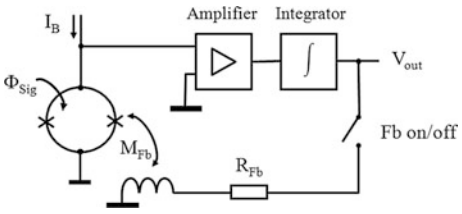

Fig. 8 Schematics of a directly coupled SQUID electronics. R_{Fb} and M_{Fb} denote the feedback resistor and mutual inductance between feedback coil and SQUID, respectively. In feedback mode the output voltage V_{out} is linearly dependent on the external signal flux Φ_{Sig}

$$\sqrt{S_{\Phi,t}} = \sqrt{\left(\sqrt{S_{\Phi,SQ}}\right)^2 + \left(\frac{\sqrt{S_{V,Amp}}}{V_\Phi}\right)^2 + \left(\sqrt{\frac{S_{I,Amp} \cdot R_{dyn}}{V_\Phi}}\right)^2}. \quad (18)$$

Here $S_{\Phi,SQ}^{1/2}$ is the intrinsic flux noise of the SQUID, $S_{V,Amp}^{1/2}$ and $S_{I,Amp}^{1/2}$ are the preamplifier input voltage and current noise, respectively. R_{dyn} denotes the dynamic SQUID resistance in the working point.

Typical input voltage and input current noise of state-of-the-art SQUID electronics are about 0.35 nV/Hz$^{1/2}$ and (2–6) pA/Hz$^{1/2}$ [41, 42]. For currently available dc SQUIDs the usable voltage swing and transfer function can typically vary between (30–150) μV and (100–500) μV/Φ_0, respectively. The dynamic resistance of such SQUIDs is usually between 5 and 50 Ω. As a result, the contribution of the room-temperature SQUID electronics can amount up to (1 − 5) μΦ_0/Hz$^{1/2}$ and may thus considerably contribute to the total measured flux noise. In part two of this section we will comment on possible noise-reduction techniques.

Note that the expression above does not account for the noise contribution due to thermal noise in the feedback resistor, given by $S_I^{1/2} = (4k_BT/R_{Fb})^{1/2}$. This current noise converts into flux noise in the SQUID via the mutual inductance M_{Fb}. Especially in SQUID systems requiring a large dynamic range, for example for unshielded operation within the Earth's magnetic field, this noise, however, may become important or even dominant.

Since SQUIDs are vector magnetometers, a rotation in the Earth's field results in a field difference[2] of up to 130 μT. Thus a SQUID magnetometer system with magnetic field noise of for example 10 fT/Hz$^{1/2}$ would require a dynamic range of the order of 200 dB which is larger than 30 Bit.[3] Even if the SQUID electronics would allow such an operational range, current analogue to digital converters (ADC) are nowadays still limited to about 24 Bit.

Besides the dynamic range, another important parameter correlated with the dynamic behavior of the FLL is the system slew rate [39, 41] given by

$$\dot{\Phi}_{\max} = \left|\frac{\partial \Phi_{Fb}}{\partial t}\right| = 2\pi \cdot f_{GBP} \cdot \delta V \cdot \frac{M_{Fb}}{R_{Fb}}. \quad (19)$$

It describes the maximum signal change in a certain time interval that the electronics is able to follow. Here f_{GBP} is the gain-bandwidth product, a fixed value for a specific amplifier configuration and δV describes the usable voltage swing of the SQUID. Accordingly, a high system slew-rate demands a large δV and a small feedback resistor value, which however may limit the system noise. The

[2]Depending on the location on Earth and taking into account only the crustal contribution of the Earth's magnetic field.

[3]In a 1 Hz bandwidth, the dynamic range can be calculated as $DR = 20 * \log$ (130μT/10fT/Hz$^{1/2}$*crest factor). Taking a crest factor of 4 this results in $DR = 190$ dB > 30 Bit.

configuration of the feedback circuit is therefore always a tradeoff between low system noise and high dynamic range and slew rate.

2.3.2 Noise-Reduction Techniques

As pointed out before, the noise contribution of the electronics may become dominant even with state-of-the-art SQUID electronics. It is obvious that increasing the transfer function V_Φ results in a reduction of this contribution.

In order to raise V_Φ of the SQUID, a readout scheme known as additional positive feedback (APF) was proposed by Drung et al. [43]. It consists of a resistor R_{APF} with an inductor L_{APF} in series, which are connected in parallel to the SQUID, as shown in Fig. 9. The incorporated inductor L_{APF} is magnetically coupled to the SQUID. In a working point on the positive slope of the flux-voltage characteristics a small signal $\delta\Phi$ will produce a positive voltage δV. Accordingly, the current through the APF coil will increase and will thus enlarge the SQUID voltage further. As a result, the flux-voltage characteristic is steepened at the positive slope, whereas the negative slope will be decreased, as illustrated in Fig. 9.

This L_{APF}-R_{APF} circuit acts as a small signal preamplifier and the transfer function V_Φ will be increased on the positive slope of the flux-voltage characteristics. The effect of the input voltage noise of the preamplifier is therefore reduced. This enhancement in V_Φ comes along with a reduction in the usable voltage swing of the SQUID and it reduces the linear flux working range Φ_{lin}. It is thus unfavorable for systems needing a large slew rate [39]. In such a configuration R_{APF} will as well contribute to the total measured noise.

Another way to decrease the contribution of the room temperature SQUID electronics is to use a second SQUID as a low noise preamplifier [44]. Figure 10 illustrates such a two-stage setup. Here, the SQUID to be measured (SQ_1) is typically operated in voltage bias mode ($R_C \ll R_{dyn}$) and the current modulation due to

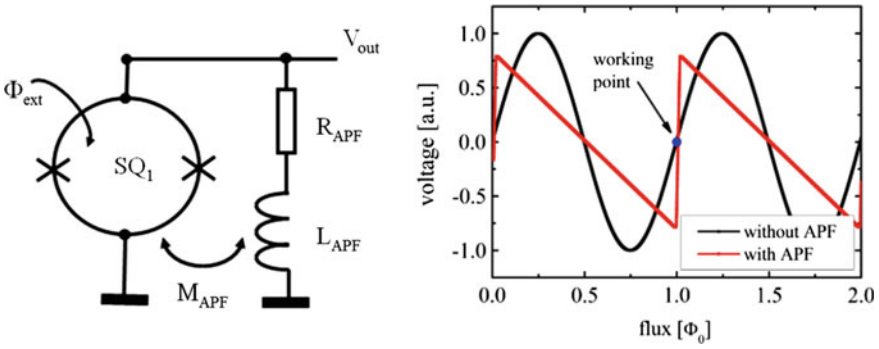

Fig. 9 Schematics of the additional positive feedback (APF) circuit. The flux-voltage characteristic with APF is steepened at the positive slope compared to the characteristics without APF. Note that the usable voltage swing across the SQUID decreases for APF

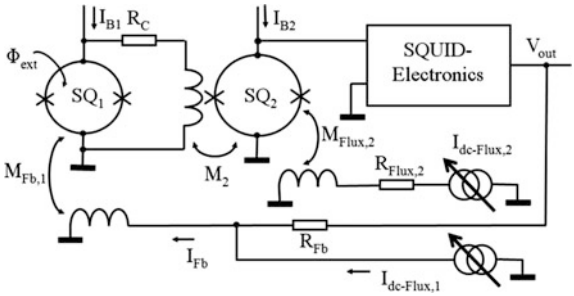

Fig. 10 Schematics of a two-stage measurement setup. The current modulation of SQUID SQ_1 due to an external signal flux Φ_{ext} is sensed in an amplifier SQUID SQ_2. Feedback may be applied to the first stage SQUID (as shown in the figure) or to SQUID SQ_2, when operated as a voltmeter

an external signal is sensed in an amplifier SQUID SQ_2. An appropriate choice of the mutual input coil inductance M_2 of the amplifier SQUID sets the flux gain $G_\Phi = (\partial\Phi_2/\partial\Phi_1)$ between the two SQUID stages to a sufficient level. The overall noise of the two-stage configuration using a directly coupled SQUID electronics amounts to [39]

$$\sqrt{S_\Phi} = \sqrt{\left(\sqrt{S_{\Phi,1}}\right)^2 + \frac{1}{G_\Phi^2}\left[\left(\sqrt{S_{\Phi,2}}\right)^2 + \left(\frac{\sqrt{S_{V,Amp}}}{V_{\Phi,2}}\right)^2 + \left(\sqrt{\frac{S_{I,Amp}\cdot R_{dyn,2}}{V_{\Phi,2}}}\right)^2\right]}. \tag{20}$$

The subscripts 1 and 2 denote SQUID SQ_1 and SQ_2 respectively.

Obviously, a large flux gain allows neglecting the contribution of the amplifier SQUID and the FLL. Especially in cases where the front-end SQUID SQ_1 is operated at a very low temperature $T \ll 4.2$ K, the two-stage configuration is often the only way to make use of the low level of SQUID noise. However, in such a configuration the linear flux-range and thus the system slew rate are reduced.

To increase the voltage signal and thus the transfer function without affecting the linear flux range, a so-called series SQUID array with many identical SQUIDs connected in series can be used. If the deviation in the critical currents of the SQUIDs is low enough and provided that the same flux is coupled to all SQUIDs in the array, the voltage modulations of the individual SQUIDs coherently sum up to a single SQUID-like characteristic. For a series array of N SQUIDs the transfer function and flux noise are given by

$$V_{\Phi,Array} = N \cdot V_{\Phi,SQ} \text{ and} \tag{21}$$

$$\sqrt{S_{\Phi,Array}(f)} = \sqrt{S_{\Phi,SQ}(f)}/\sqrt{N}. \tag{22}$$

Obviously, the flux noise of a SQUID array can become considerably smaller than for a single SQUID. The direct use of series SQUID arrays as a current sensor coupled to a pickup loop with the purpose of measuring the flux induced screening current is, however, not feasible, as inevitable inaccuracies in the lithography and hence small variations in SQUID geometries lead to amplitude modulation of the flux-voltage characteristics for large flux bias values. Trapped flux in the individual SQUIDs of the array may as well cause distortions in the flux-voltage characteristics.

SQUID arrays are therefore often used as amplifier SQUIDs in a two-stage configuration as discussed above. As the flux noise scales with $N^{1/2}$, even a moderate number N of SQUIDs and a low flux gain may be sufficient for most applications. In Refs. [45, 46] the use of series SQUID arrays as readout devices for SQUIDs has been shown. They achieved output voltages in the mV range and bandwidths of more than 100 MHz.

Instead of a series array, which provides a periodic flux-voltage characteristic, a series connection of intentionally different SQUIDs with an appropriate distribution of SQUID inductances show only one pronounced minimum [47, 48]. These devices are known as superconducting quantum interference filter (SQIF). Although this scheme shows somewhat higher noise than series SQUID arrays with the same number of individual SQUIDs, it may be advantageous for some applications since locking to multiple working points in the amplifier SQUID in FLL mode is not possible.

Let us conclude this section with a more general comment: nowadays SQUID electronics have become mature and offer low noise and large bandwidth combined with low thermal drift, low power consumption and small size, allowing to operate SQUID systems even in remote areas. They are typically computer controlled with an automated setup of SQUID working points and there even exist user-friendly one-button solutions. The current trend is towards a higher speed and bandwidth or the integration of preamplifier stages (also SQUID based) at 4.2 K to avoid the delay times due to signal propagation in the connecting wires between room-temperature and the cryogenic bath.

3 SQUID Fabrication

The fabrication of LTS SQUIDs is based on sophisticated thin-film techniques similar to their use in semiconductor industry. SQUID sensors are fabricated on wafers, which are then diced into chips with dimensions of several mm^2 size depending e.g. on the necessary pickup area for the envisaged application. Quartz, silicon or oxidized silicon wafers sized 4 inch or larger are typically used as substrates. Therefore, hundreds of SQUIDs can be fabricated in one run.

In this section we will comment on basic thin-film techniques used for the fabrication of LTS SQUIDs and we will highlight the most important step, the junction fabrication. More detailed information can e.g. be found in [49].

3.1 Lithography and Thin-Film Techniques

Nowadays superconducting thin film materials for LTS SQUIDs are mainly Nb and Al. In the beginning usually Pb or Pb alloys have been used (as well as electrode material for the junction fabrication), but the limited long term stability and problems associated with thermal cycling have led to the "all-refractory" process used today.

To fabricate thin superconducting films, various deposition techniques such as thermal or e-beam evaporation, molecular beam epitaxy, plasma and ion beam sputtering can be used. Due to the high melting temperature of Nb, sputtering is de facto the standard. This is typically done in ultra-high vacuum, as impurities may dramatically change the superconducting thin-film properties.

A careful optimization of the deposition and patterning process of superconducting films with respect to their influence on e.g. minimum film stress, superconducting properties or the shape of the structured edges is essential. Steep edges of superconducting films are usually favorable, as they are less susceptible to flux trapping. In multilayer processes, moreover, special attention has to be paid to avoid residues or fence structures associated with the patterning of the films as they may lead to shortcuts in or failure of the devices. Higher integrated multilayer processes like the Josephson junction based rapid single flux quantum (RSFQ) logic [50, 51] try to overcome difficulties associated with an increased number of superconducting layers and therefore potential step height or surface topography problems by planarization of isolation layers (typically with chemical mechanical polishing). As the design of SQUIDs is usually less complex than RSFQ circuits, planarization is in generally not performed in SQUID fabrication nowadays, but it may be implemented in future.

The patterning of the thin films is either done by lift-off or by etching. For lift-off, the photoresist is applied to the substrate prior to the thin film deposition. When the thin film is patterned via etching, the photoresist is placed on top of the thin film. In both cases the resist acts as a mask for the structure to be defined. For lift-off the resist is removed in an (ultrasonic) solvent bath so that the film on top of the resist is removed as well. The etch process is typically done by dry etching such as plasma or reactive ion-beam etching. Wet etching may as well be used, but is not that attractive due to the isotropic etch behavior. To avoid over-etching of the underlying film, one can either use an end-point detector or make use of thin natural etch stops like an Al layer for a fluorine based etch process.

In general, elevated temperatures should be avoided (especially when the trilayer to form the Josephson junctions is already deposited on the wafer), as this increases e.g. the diffusion of hydrogen into the thin film or may change the barrier characteristics [52, 53].

The typical film thickness is in the range of 50 to about 300 nm. The linewidth of superconducting structures such as patterned multi-turn input coils on top of the SQUID washer may be as small as 1 μm or even less. The resist thickness depends

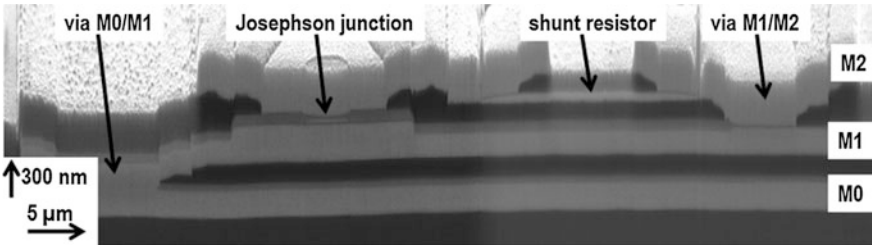

Fig. 11 Scanning electron microscope image of the cross-section of a shunted Nb–AlO_x–Nb Josephson junction. The sample was prepared by focused ion beam etching. M0, M1 and M2 indicate the different Nb wiring layers. The *vias* are interconnects between these layers. Reprinted from Reference [54], reproduced with permission of Elsevier

on the lithography method and the lateral dimension of the desired thin film structure and may vary between several hundred nm to about 2 µm.

Depending on the design complexity, the fabrication of LTS SQUIDs includes at least 2 superconducting layers, one for the SQUID washer and one for the input and feedback coils, and (several) isolation layers. Figure 11 shows a scanning electron microscope image of a cross-section of a shunted Josephson junction together with the appropriate Nb wiring layers used in the Fluxonics foundry RSFQ process [54].

3.2 Junction Fabrication

Nowadays SIS Josephson junctions are typically based on a sandwich of an in situ deposited Nb–AlO_x–Nb trilayer. There are other material systems like e.g. Nb–SiN_x–Nb but they do not exhibit such a good junction quality, reproducibility, low junction capacitance, and low level of critical current fluctuations. Detailed information on other material systems used in the past can be found in [49, 55].

Today, most fabrication technologies are based on the so-called SNAP process (selective niobium anodization process) [56] or its numerous variations. In 1983 Gurvitch introduced the use of Nb–AlO_x–Nb Josephson junctions [57]. This material combination has led to superior junction characteristics and became soon the most important junction fabrication process. Up to now it is the standard even for very complex RSFQ circuits for digital applications and it allows the reliable fabrication of up to tens of thousands Josephson junctions on a single chip [50].

The junction fabrication starts with the deposition of a trilayer consisting of a Nb base electrode, a thin Al layer (which is partly oxidized during the trilayer deposition) and another Nb layer as counter electrode. The in situ deposition of the trilayer is essential for clean interfaces between these layers. The AlO_x is formed by exposing the sputtered Al to pure oxygen atmosphere for a certain time. The thickness of the AlO_x layer t_{ox}—given by the product of oxygen partial pressure and exposure time—determines the junction's critical current density j_C, which is

exponentially dependent on t_{ox}. For SQUIDs j_C is in the range of (0.1–2) kA/cm^2 depending on the desired junction's critical current and size. The typical film thickness is (50–300) nm for Nb layers and about 10 nm for Al. The thin Al layer is used to level out the surface roughness of the underlying Nb layer and allows a low junction capacitance due to the much lower dielectric constant ε_r of AlO_x compared to NbO_x.

In the SNAP process the junction area is defined by anodizing the upper electrode of the trilayer. During anodization the desired junction area is covered by a small resist dot. In this so-called window-type process the typical minimum junction size is several μm^2. Since the anodization solution creeps partly under the photoresist, small junctions are less reproducible or even defective.

For electrical connection of the junction a Nb layer is deposited on top of the counter electrode. Finally a shunt resistor is placed close to the junction to damp its dynamics and to fulfil the condition $\beta_C \leq 1$. Usually Pd, AuPd, Ti, or Mo is used as shunt material. Figure 12 (left) shows a scanning electron microscope image of such a window-type junction with dimensions of (3 × 3) μm^2.

The specific capacitance of a Nb–AlO_x–Nb Josephson junction (it forms a parallel-plate capacitor) is about 45–60 fF/μm^2, depending on the barrier thickness and therefore on the critical current density [58]. Due to the overlap of superconducting layers around the junction (e.g. to compensate inevitable alignment errors between different layers), a parasitic capacitance is formed, which adds to the junction capacitance. The influence of this effect becomes even more pronounced as the junction size is reduced.

As discussed in Sect. 2.2, a small total junction capacitance is favorable since it will improve the performance in terms of energy resolution and voltage swing of the SQUID. To reduce or even avoid parasitic capacitance, several fabrication technologies have been reported. One possible approach is the so-called cross-type technology [59], in which the junction is defined by the overlap of two narrow

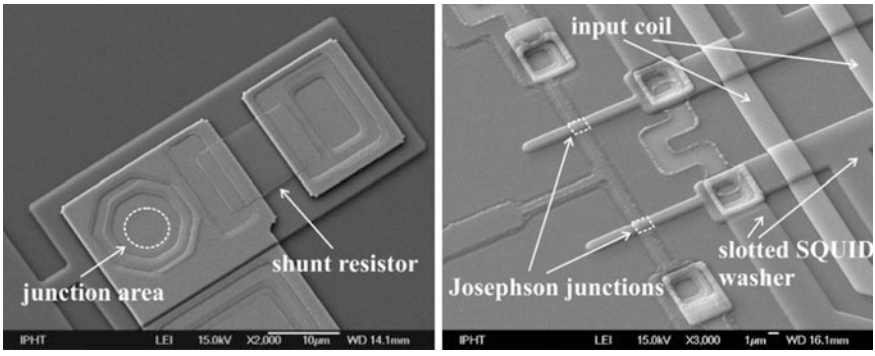

Fig. 12 (*Left*) Scanning electron microscope (SEM) image of a Josephson junction fabricated in the window-type technology and (*Right*) SEM image of a SQUID fabricated in the cross-type junction technology. In this technology the junction size is considerable reduced and parasitic capacitances due to the overlap of superconducting layers around the junction is avoided

perpendicular strips. Figure 12 (right) shows a SEM image of the central SQUID part with the Josephson junctions as indicated. The lower strip is the entire Nb–AlO_x–Nb trilayer, which is patterned with the width corresponding to the desired linear dimension of the junction. The second perpendicular strip of Nb is deposited on top of the trilayer and acts as a mask for patterning the Nb counter electrode from the trilayer. Due to the self-alignment of the process, no parasitic capacitance is formed. In [59], high quality Josephson tunnel junctions with dimensions of $(0.6 \times 0.6)\ \mu m^2$ have been reported. Due to the narrow linewidth design of the junctions, flux trapping is avoided and these devices can be cooled in the Earth's magnetic field without restrictions [60].

The current trend in superconducting fabrication technology is the further decrease in junction capacitance and accordingly a downsizing of the Josephson junctions, while maintaining a high fabrication yield and low parameter spread over the entire wafer.

4 State-of-the-Art Devices

As discussed above, SQUIDs can be used not only as magnetometers, but also as sensors for any physical property that can be transformed into magnetic flux. In this section we will show results achieved with state-of-the-art devices aimed for a number of applications.

4.1 SQUID Magnetometer

For a SQUID magnetometer the figure of merit is the equivalent magnetic field noise $S_B^{1/2} = S_\Phi^{1/2}/A_{eff}$. As we have seen, for optimized SQUID parameter β_L and β_C of about unity, the flux noise $S_\Phi^{1/2}$ can be expressed as a function of the design dependent parameters SQUID inductance L_{SQ} and junction capacitance C_{JJ}. For the smallest junction size in the used fabrication process, the optimization with respect to low $S_B^{1/2}$ can be carried out by minimizing the ratio L_{SQ}/A_{eff}. It describes how effective a given SQUID inductance—which determines the magnitude of white flux noise—is transformed into an effective area.

As already discussed above, multiloop magnetometers allow for the best field resolution for a given chip area. Excellent results have been achieved, yielding in magnetic field noise levels of below 1 $fT/Hz^{1/2}$ in the white noise region [36, 61]. Figure 13 (left) shows a field noise spectrum of a device with an outer pickup coil dimension of 12 mm. The devices show a typical white field noise of about 0.3 $fT/Hz^{1/2}$.

SQUID magnetometers may also be realized by connecting a thin-film or wire wound pickup coil to the input coil of a current sensor SQUID. As discussed in Sect. 2.2, the magnetic field noise can be improved by increasing the pickup loop

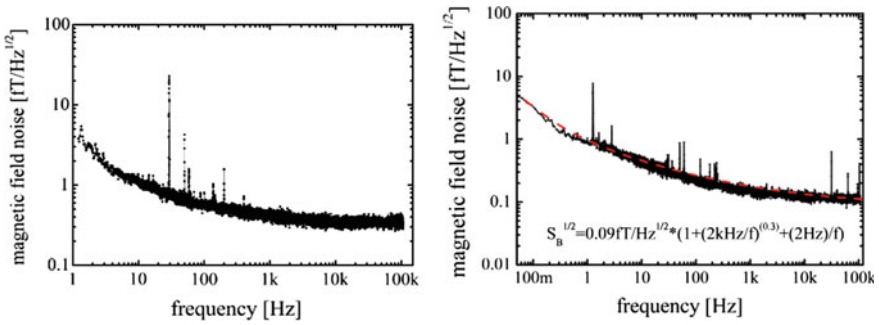

Fig. 13 (*Left*) Field noise spectra of an integrated multiloop magnetometer SQUID with an outer pickup coil dimension of 12 mm and (*Right*) of a magnetometer composed of a SQUID current sensor and an all thin-film pickup coil with dimensions of (29 × 33) mm^2. The *left figure* is reprinted from Reference [61], reproduced with permission of IOP Publishing Ltd

area, while maintaining $L_{in} \approx L_p$. Limitations of this approach are e.g. due to the inner cryostat dimensions or noise arising from impurities in the dewar walls or the used superinsulation around the dewar. The SQUID system should moreover feature a sufficiently large dynamic range for the intended application.

Figure 13 (right) shows a magnetic field noise spectrum of a SQUID magnetometer composed of a highly sensitive SQUID current sensor connected to a thin-film pickup coil with dimensions of (29 × 33) mm^2. The device exhibits a white field noise level of about 0.1 fT/Hz$^{1/2}$, showing excellent agreement with the rough approximations in Sect. 2.2. It is worth to note that $S_B^{1/2}$ is still below 1 fT/Hz$^{1/2}$ at 1 Hz.

Both spectra in Fig. 13 show a shallow increase of the noise starting at frequencies of about 10 kHz, which is caused by magnetic flux noise as discussed in Sect. 2.2. If this source of noise is identified, further noise improvement in the frequency range 1 Hz $< f <$ 10 kHz may be expected. At frequencies below about 1 Hz, noise arising from critical current fluctuations in the Josephson junctions became dominant, as can be seen in Fig. 13 (right).

Beside the superior noise performance of the devices, which is usually measured inside a high-permeable and superconducting shielding, the performance of the SQUID system in unshielded operation is of particular importance. In e.g. [62] the noise of a SQUID system cooled and operated in the Earth's magnetic field has been investigated. The system noise is estimated by correlating the signal of two identical SQUID systems aligned in parallel to cancel out natural geophysical noise. Figure 14 (left) shows the spectrum from raw data of these two systems. As could be seen, there is an excellent correlation between the channels in parallel, allowing to use the discussed correlation techniques.

Figure 14 (right) shows the estimated intrinsic noise by cross-correlation in the frequency domain. The according white system noise is about (1.2–1.5) fT/Hz$^{1/2}$ for the three orthogonal channels. The estimated low-frequency noise may not represent the intrinsic system noise due to a small misalignment between the two

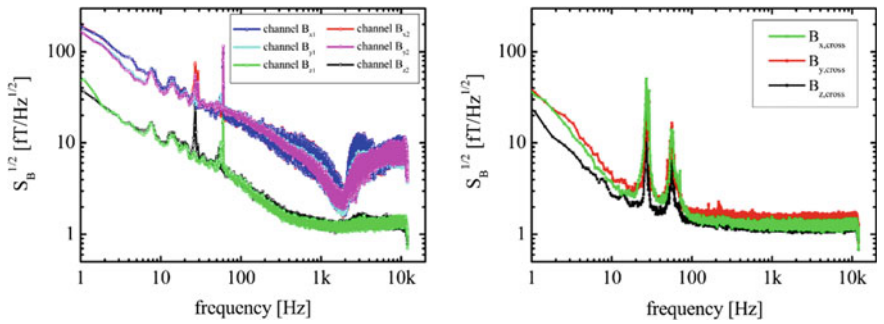

Fig. 14 (*Left*) Spectra of two highly sensitive SQUID systems, each comprising three orthogonal SQUIDs. Unshielded measurement was performed simultaneously NW of Delta, Utah, USA. (*Right*) Estimated intrinsic SQUID system noise obtained by a cross-correlation technique in the frequency domain from the raw data as shown *left*. Reprinted from Reference [62], reproduced with permission of IOP Publishing Ltd

systems and probably due to noise induced by motion of the system in the Earth's magnetic field.

4.2 Gradiometer

As we have discussed in Sect. 2.3, the mobile operation of such highly sensitive SQUID magnetometers in the Earth's magnetic field would require a dynamic range exceeding 30 Bit, well beyond the capability of current electronics and AD converter. If the pickup loop is configured as a gradiometer with two or more coils of opposite winding arranged at a certain baseline, distant (noise) sources do not produce a signal in the input coil since they produce spatially very homogeneous fields. Signals from a nearby sample, however, produce a spatially inhomogeneous field at the gradiometric pickup loop, leading to a signal current in the loop, which will be detected by an inductively coupled SQUID current sensor [63].

The quality of the gradiometer is usually denoted as the balancing, that is the gradiometer response to a homogenous magnetic field. For an ideal gradiometer there is no response, as the effective areas of opposite windings of the input coil are equal. As inaccuracies in e.g. the lithography cannot be avoided, real devices exhibit (small) parasitic areas to a homogenous magnetic field. Thus, in a gradiometer system all components of the magnetic field are usually measured simultaneously to allow for a compensation of the residual imbalance.

There are in principle two classes of gradiometers: electronic and intrinsic gradiometers. In electronic gradiometers, the FLL output voltages of two SQUID magnetometers separated by a certain baseline are subtracted. However, the sensitivity of such SQUIDs, and therefore of the gradiometer, is typically low due to dynamic range issues as discussed for magnetometers operating in the Earth's

magnetic field. To reduce the dynamic range requirements, these two magnetometers may be operated within a global feedback scheme [64].

Intrinsic gradiometers directly measure the difference of magnetic fields threading two pickup-loops. Typically a serial connection of two pickup loops, which are arranged in a figure of eight, is used. The pickup loop may consist of a thin film or be wire wounded, and is connected to the input coil of a SQUID current sensor. In this case the SQUID should be arranged as a second order gradiometer to solely measure the flux induced by the screening current in the pickup loop.

Depending on the component of the magnetic field gradient tensor $G_{i,j} = \{\partial B_i / \partial x_j\}$ (with $i,x_j \in \{x, y, z\}$) that should be measured, either planar or axial type gradiometers are used. Planar type gradiometers are often integrated all thin-film devices, as this allows for better balancing, which is ideally limited just by lithography alignment errors. In their axial counterparts usually a wire wound pickup coil is used.

With an appropriate balance of the gradiometer, they allow for a mobile operation within the Earth's magnetic field, without exceeding the dynamic range of current feedback circuits. Thus, they enable to measure the complete magnetic gradient tensor with high sensitivity. Sophisticated inversion algorithms may thus enable the detection and probably a localization of the signal source.

Figure 15 shows a noise spectrum of a planar integrated all thin-film SQUID gradiometer. The gradiometer has a baseline of 40 mm and a gradiometric pickup loop shaped in a figure of eight with a size of the two loops of each (20 × 20) mm^2. The white noise amounts to 18 $fT/mHz^{1/2}$. These integrated devices show a balance of about 1×10^4. Using the simultaneously acquired magnetic field components to compensate for the measured parasitic areas, a balance of up to 1×10^7 has been achieved [65].

4.3 Current Sensors

For SQUID based current sensors typically an integrated superconducting input coil is placed on top of the SQUID washer. The input coil is inductively coupled to the

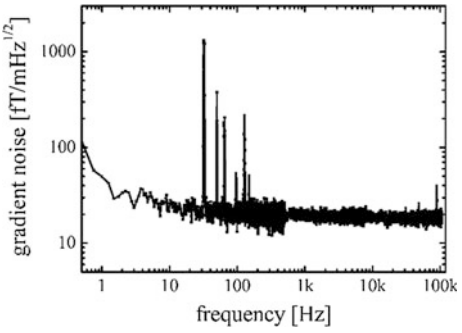

Fig. 15 Noise spectrum of a planar SQUID gradiometer measured inside a magnetic shielding. The gradiometer baseline is 40 mm and the size of the two pickup loops is (20 × 20) mm^2 each. The measured white gradient noise is 18 $fT/mHz^{1/2}$

SQUID loop, so that a current in this coil produces a magnetic flux inside the loop. It therefore can be used as a current sensor with inductive input impedance.

Tight coupling of the input coil allows for a good current resolution $S_I^{1/2} = S_\Phi^{1/2}/M_{in}$. Since the mutual input inductance M_{in} is proportional to the SQUID inductance and the number of turns on the SQUID washer, many turns need to be integrated depending on the required current resolution. Limitations arise from the minimum linewidth and distance between adjacent windings given by the fabrication process. Moreover, the superconducting properties of the input coil need to be preserved: the superconducting thin film needs sufficient edge coverage so that the signal current does not exceed the critical current of the thin film.

However, tight coupling of an integrated input coil may lead to strong resonances in the flux-voltage characteristics and demands for a throughout sensor optimization, as discussed in Sect. 2.2. Another possibility to effectively couple an input coil with a few μH to a SQUID with an inductance of about 100 pH or less is to make use of a double-transformer coupling scheme [66]. Here, an additional intermediate flux transformer is used, which may be a thin-film variant, which may as well be located on a separate chip or a wire wound transformer typically used e.g. for cryogenic current comparators [67].

In [68] a wire wound current comparator having 10,000 turns in the primary coil is reported, achieving a current resolution of 4 fA/Hz$^{1/2}$ in the white noise region. Integrated thin-film devices are in most cases preferable to their bulky wire wound counterparts and recently white noise levels of about 110 fA/Hz$^{1/2}$ [69], 25 fA/Hz$^{1/2}$ [70] and 3 fA/Hz$^{1/2}$ [71] have been achieved.

Figure 16 shows the noise spectrum of the device described in [71]. The white current noise amounts to 3 fA/Hz$^{1/2}$. It consists of a SQUID chip with dimensions of (2.5 × 2.5) mm^2 and separate flux-transformer chips of (12.5 × 12.5) mm^2. With the measured input inductance of 9.5 mH the energy resolution can be estimated to about 65 h.

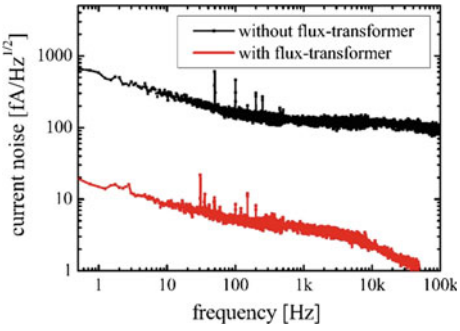

Fig. 16 Noise spectra of the SQUID current sensor with and without the transformer normalized to the input current. The white noise amounts to 3 fA/Hz$^{1/2}$ and 110 fA/Hz$^{1/2}$ with and without transformer, respectively. Reprinted from Reference [71], reproduced with permission of IOP Publishing Ltd

4.4 Further Applications and Trends

4.4.1 Miniature and Nano-SQUIDs

In contrast to SQUID magnetometers, which are usually aimed for a low magnetic field noise, miniature or even nanometer sized SQUIDs or SQUIDs with pickup loops in this dimension are optimized for a good spatial resolution and low noise. They may be used for SQUID microscopy [22] or as miniature SQUID susceptometers [14].

Current research focuses e.g. on the application of such sensors for the investigation of small spin systems and the detection of single electron spin-flips [72–74].

In order to improve the spin sensitivity $S_\mu^{1/2} = S_\Phi^{1/2}/\Phi_\mu$ of such SQUIDs (here S_μ and S_Φ are the noise spectral power density normalized to the magnetic moment and flux, respectively), one needs to reduce their physical dimensions, thereby reducing the equivalent flux noise spectral density S_Φ via the decrease in total SQUID inductance L_{SQ}, as well as increasing the coupling Φ_μ between a particle with magnetic moment μ to the SQUID [14, 75].

Miniaturized SQUIDs are usually realized using constriction type junctions, where a small hole is patterned into a thin superconducting strip either by electron beam or focused ion beam lithography [76–79]. In [80] a nano-SQUID has been realized by depositing a SQUID loop on the apex of a hollow quartz tube pulled into a very sharp pipette. For Pb based devices white flux noise levels of down to 50 $n\Phi_0/Hz^{1/2}$ have been reported.

The above presented cross-type Josephson tunnel junctions allow for the implementation of SIS junctions that are preferred compared to their SNS (superconductor-normal conductor-superconductor) counterparts [81]. Their small junction capacitance results in a remarkable reduction of white flux noise levels. Figure 17 shows a scanning electron micrograph of a device with an inner loop dimension of 1.5 μm. The right panel of Fig. 17 shows the flux noise spectrum of a device with 0.5 μm loop dimension. From the measured white flux noise of about 70 $n\Phi_0/Hz^{1/2}$ a spin sensitivity of $S\mu^{1/2} < 7\mu_B/Hz^{1/2}$ has been estimated [82].

4.4.2 Emerging SQUID Concepts

To overcome the problems associated with the dynamic range of SQUID systems and limited resolution of current AD converters, several SQUID concepts have been introduced, with e.g. digital feedback loops operated either at room temperature [83, 84] or integrated on the sensor chip [85, 86]. These so-called digital SQUIDs are usually based on a critical current comparator in a superconducting pickup loop. Here, the screening current due to an external flux threading the pickup loop is

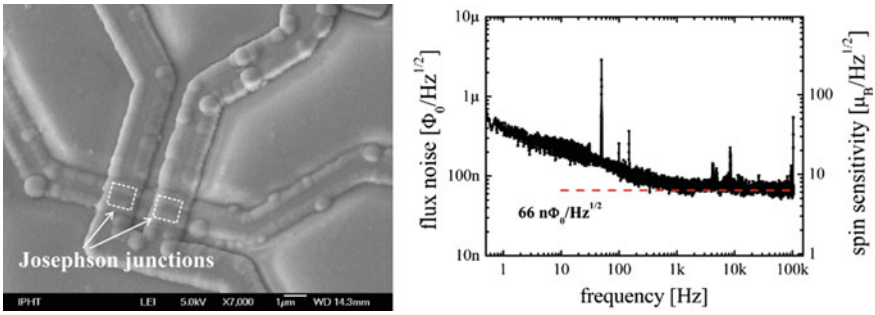

Fig. 17 (*Left*) Scanning electron micrograph of a miniaturized SQUID with an inner loop dimension of 1.5 μm based on cross-type Josephson junctions. (*Right*) Flux noise spectrum of a nanoSQUID with 0.5 μm loop dimension. The equivalent white flux noise corresponds to 66 $n\Phi_0/Hz^{1/2}$. The spin sensitivity (right hand axis) was calculated according to $S_\mu^{1/2} = S_\Phi^{1/2}/\Phi_\mu$, with the estimated coupling $\Phi_\mu = 10.5\ n\Phi_0/\mu_B$. Reprinted from Reference [82], reproduced with permission of IOP Publishing Ltd

superimposed to the bias current of e.g. a hysteretic single Josephson junction. If the sum of both exceeds the junctions critical current, it switches to the voltage state. Applying an ac-bias allows to reset the hysteretic junction and further enables the up and down-counting of the flux in the loop. The single junction may be replaced by a magnetically coupled SQUID to increase the current sensitivity and to avoid a direct feedback to the pickup loop.

The integration of on-chip Josephson junction logic like RSFQ avoids the time delay due to signal propagation to the room-temperature electronics and enables data pre-processing. Thus, large bandwidths of several 100 MHz and large system slew-rates may become possible. First prototypes of such SQUIDs have been fabricated, but the reliable low-noise operation has to be proven in practical applications. However, the on-chip integration is accompanied by a strong increase in circuit complexity and thus greater demands on the fabrication process.

In [87], another operation principle has been introduced to overcome the dynamic range limitation of current SQUID systems. In this configuration, a cascade of coplanar SQUIDs, which exhibit effective areas differing by several orders of magnitude, are arranged on a single chip. Assuming a homogenous magnetic field over the chip area, the information is thus split into several channels, which are digitized individually. Information is composed by post-processing of the data. Figure 18 illustrates the cascade principle. The correct branch of the sensitive SQUID is determined by a reference SQUID which operates in its own feedback loop. The sensitivity of the SQUID system is given by the most sensitive SQUID in the cascade. In [87] an overall dynamic range of 190 dB has been reported. The presented SQUID system, moreover, enables the absolute measurement of the vector components of the Earth's magnetic field.

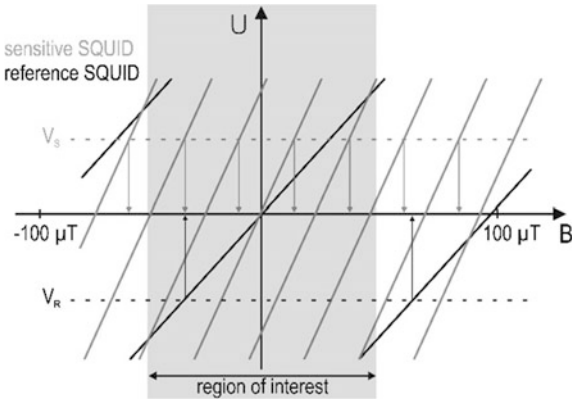

Fig. 18 Working principle of the SQUID cascade setup: In the region of interest, the reference SQUID exhibits a unique operating point. The output voltage of this reference SQUID V_R then indicates the possible working range of the sensitive SQUID, which determines the overall system sensitivity. Reprinted from Reference [87], reproduced with permission of IOP Publishing Ltd

5 Concluding Remarks and Outlook

SQUIDs are today's most sensitive devices for the detection of magnetic flux with energy resolutions approaching the quantum limit. They have a wide and flat frequency response ranging from dc to several GHz. SQUIDs can be used as sensors for any physical quantity that can be transformed into magnetic flux, such as current, voltage, magnetization and susceptibility, displacement as well as temperature and others. They are therefore very versatile and can address a large variety of applications.

To exploit the superior sensitivity of LTS dc SQUIDs, however, a low operation temperature, of 4.2 K and below is mandatory. The need for cryogenics is a significant barrier to the widespread application of SQUIDs since both the operator's convenience and the system costs are impaired. In this context we would like to recall the comment of Harold Weinstock given at a NATO Advanced Study Institute in 1990: "Never use a SQUID when a simpler, cheaper device will do the job."

Fortunately, during the last years, general demand has advanced the development of cryocoolers which are now commercially available in a variety of models. However, to use these mechanical coolers, the measurement chamber is typically magnetically shielded, to attenuate magnetic and vibrational noise from the cryocooler. If these noise sources can be reduced considerably at reasonable expenses, a variety of potential markets may be opened.

The fabrication of LTS SQUIDs based on Nb–AlO_x–Nb Josephson junctions is already a mature technology and allows the reliable fabrication of up to tens of thousands Josephson junctions on a single chip. Current technology development is

mainly towards a further decrease in junction capacitance and accordingly a downsizing of the Josephson junctions, as well as yield and parameter spread optimization. This will result in a strong sensitivity increase of SQUIDs. Moreover, small linewidth devices enable the operation in ambient magnetic fields. Revealing the origin of magnetic flux noise may further improve the sensitivity of modern SQUIDs.

During the last years, SQUID electronics have been developed towards low noise and large bandwidth together with low thermal drift, low power consumption and small size. User-friendly solutions that can be operated even by non-professional personal are available. Current research focuses towards a higher speed and further increased bandwidth and the integration of preamplifier stages at 4.2 K. A significant increase in dynamic performance—a key issue especially for highly sensitive unshielded mobile operation—may be expected.

Acknowledgements The authors highly acknowledge Dr. S. Anders for careful proofreading and many stimulating discussions.

References

1. M. Tinkham, *Introduction to Superconductivity* (Dover Publications, USA, 1996)
2. W. Buckel, R. Kleiner, *Superconductivity* (Wiley-VCH, Weinheim, 2008)
3. H. Weinstock, *Squid Sensors: Fundamentals, Fabrication, and Applications* (Kluwer Academic Publishers, Dordrecht, 1996)
4. J. Clarke, A.I. Braginski, *The SQUID Handbook: Fundamentals and Technology of SQUIDs and SQUID Systems* (Wiley-VCH, Weinheim, 2004)
5. J. Clarke, A.I. Braginski, *The SQUID Handbook: Applications of SQUIDs and SQUID Systems* (Wiley-VCH, Weinheim, 2006)
6. P. Seidel, *Applied Superconductivity: Handbook on Devices and Applications* (Wiley, Hoboken, 2015)
7. R. Jaklevic, J. Lambe, A. Silver, J. Mercereau, Quantum interference effects in Josephson tunneling. Phys. Rev. Lett. **12**, 159–160 (1964)
8. B.D. Josephson, Possible new effects in superconductive tunneling. Phys. Lett. **1**, 251–253 (1962)
9. D.E. McCumber, Effect of ac impedance on dc voltage-current characteristics of superconductor weak-link junctions. J. Appl. Phys. **39**, 3113–3118 (1968)
10. W.C. Stewart, Current-voltage characteristics of Josephson junctions. Appl. Phys. Lett. **12**, 277–280 (1968)
11. C.M. Falco, W.H. Parker, S.E. Trullinger, P.K. Hansma, Effect of thermal noise on current-voltage characteristics of Josephson junctions. Phys. Rev. B. **10**, 1865–1873 (1974)
12. R.F. Voss, Noise characteristics of an ideal shunted Josephson junction. J. Low Temp. Phys. **42**, 151–163 (1981)
13. C.D. Tesche, J. Clarke, dc SQUID: noise and optimization. J. Low Temp. Phys. **29**, 301–331 (1977)
14. M.B. Ketchen, D.D. Awschalom, W.J. Gallagher, A.W. Kleinsasser, R.L. Sandstrom, J.R. Rozen, B. Bumble, Design, fabrication, and performance of integrated miniature SQUID susceptometers. Trans. Magn. IEEE **25**, 1212–1215 (1989)
15. R.H. Koch, J. Clarke, W.M. Goubau, J.M. Martinis, C.M. Pegrum, D.J. Harlingen, Flicker (1/f) noise in tunnel junction dc SQUIDS. J. Low Temp. Phys. **51**, 207–224 (1983)

16. S. Machlup, Noise in semiconductors—spectrum of a two-parameter random signal. J. Appl. Phys. **25**, 341–343 (1954)
17. M.A. Washington, T.A. Fulton, Observation of flux trapping threshold in narrow superconducting thin films. Appl. Phys. Lett. **40**, 848–850 (1982)
18. G. Stan, S. Field, J.M. Martinis, Critical field for complete vortex expulsion from narrow superconducting strips. Phys. Rev. Lett. **92**, 097003 (2004)
19. K. Kuit, J. Kirtley, W. van der Veur, C. Molenaar, F. Roesthuis, A. Troeman, J. Clem, H. Hilgenkamp, H. Rogalla, J. Flokstra, Vortex trapping and expulsion in thin-film $YBa_2Cu_3O_{7-\delta}$ strips. Phys. Rev. B. **77**, 134504 (2008)
20. R.H. Koch, D. DiVincenzo, J. Clarke, Model for 1/f flux noise in SQUIDs and qubits. Phys. Rev. Lett. **98**, 267003 (2007)
21. M.B. Ketchen, W.J. Gallagher, A.W. Kleinsasser, S. Murphy and J.R. Clem, in *dc SQUID Flux Focused,* ed by H.D. Hahlbohm, H. Lübbig. SQUID '85—Superconducting Quantum Interference Devices and their Applications (De Gruyter, 1986), pp. 865–871
22. J.R. Kirtley, Fundamental studies of superconductors using scanning magnetic imaging. Rep. Prog. Phys. **73**, 126501 (2010)
23. J. Vrba, J. Nenonen, L. Trahms, in *Biomagnetism*, ed by J. Clarke, A.I. Braginski. The SQUID Handbook: Applications of SQUIDs and SQUID Systems (Wiley-VCH, Weinheim, 2006), pp. 269–389
24. H. Nowak, in *SQUIDs in Biomagnetism*, ed by P. Seidel. Applied Superconductivity: Handbook on Devices and Applications (Wiley, Hoboken, 2015), pp. 992–1019
25. T.R. Clem, C.P. Foley, M.N. Keene, in *SQUIDs for Geophysical Survey and Magnetic Anomaly Detection*, ed by J. Clarke, A.I. Braginski. The SQUID Handbook: Applications of SQUIDs and SQUID Systems (Wiley-VCH, Weinheim, 2006), pp. 481–543
26. R. Stolz, in *Geophysical Exploration*, ed by P. Seidel. Applied Superconductivity: Handbook on Devices and Applications (Wiley, Hoboken, 2015), pp. 1020–1041
27. R. Kraus, M. Espy, P. Magnelind, P. Volegov, *Ultra-Low Field Nuclear Magnetic Resonance: A New MRI Regime* (Oxford University Press, USA, 2014)
28. J.M. Jaycox, M.B. Ketchen, Planar coupling scheme for ultra low noise dc SQUIDs. Trans. Magn. IEEE **17**, 400–403 (1981)
29. M.B. Ketchen, Integrated thin-film dc SQUID sensors. Trans. Magn. IEEE **23**, 1650–1657 (1987)
30. J. Knuutila, M. Kajola, H. Seppä, R. Mutikainen, J. Salmi, Design, optimization, and construction of a dc SQUID with complete flux transformer circuits. J. Low Temp. Phys. **71**, 369–392 (1988)
31. R. Cantor, in *dc SQUIDS: Design, optimization and practical applications*, ed by H. Weinstock. Squid Sensors: Fundamentals, Fabrication, and Applications (Kluwer Academic Publishers, Dordrecht/Boston/London, 1996), pp. 179–233
32. J. Clarke, in *SQUID fundamentals*, ed by H. Weinstock. SQUID Sensors: Fundamentals, Fabrication and Applications (Kluwer Academic Publishers, Dordrecht/Boston/London, 1996), pp. 1–62
33. J.E. Zimmerman, Sensitivity enhancement of superconducting quantum interference devices through use of fractional-turn loops. J. Appl. Phys. **42**, 4483–4487 (1971)
34. F. Dettmann, W. Richter, G. Albrecht, W. Zahn, A monolithic thin film dc-SQUID. Physica Status Solidi (a). **51**, K185–K188 (1979)
35. P. Carelli, V. Foglietti, Behavior of a multiloop dc superconducting quantum interference device. J. Appl. Phys. **53**, 7592–7598 (1982)
36. D. Drung, S. Knappe, H. Koch, Theory for the multiloop dc superconducting quantum interference device magnetometer and experimental verification. J. Appl. Phys. **77**, 4088–4098 (1995)
37. V. Zakosarenko, L. Warzemann, J. Schambach, K. Blüthner, K.H. Berthel, G. Kirsch, P. Weber, R. Stolz, Integrated LTS gradiometer SQUID systems for unshielded measurements in a disturbed environment. Supercond. Sci. Technol. **9**, A112–A115 (1996)

38. R. Stolz, L. Fritzsch, H.G. Meyer, LTS SQUID sensor with a new configuration. Supercond. Sci. Technol. **12**, 806–808 (1999)
39. D. Drung, in *Advanced SQUID read-out electronics*, ed by H. Weinstock. SQUID Sensors: Fundamentals, Fabrication and Applications (Kluwer Academic Publishers, Dordrecht/Boston/London, 1996), pp. 63–116
40. D. Drung, Low-frequency noise in low-Tc multiloop magnetometers with additional positive feedback. Appl. Phys. Lett. **67**, 1474–1476 (1995)
41. N. Oukhanski, R. Stolz, H.G. Meyer, High slew rate, ultrastable direct-coupled readout for dc superconducting quantum interference devices. Appl. Phys. Lett. **89**, 063502 (2006)
42. D. Drung, C. Hinnrichs, H.-J. Barthelmess, Low-noise ultra-high-speed dc SQUID readout electronics. Supercond. Sci. Technol. **19**, S235–S241 (2006)
43. D. Drung, R. Cantor, M. Peters, H.J. Scheer, H. Koch, Low-noise high-speed dc superconducting quantum interference device magnetometer with simplified feedback electronics. Appl. Phys. Lett. **57**, 406–408 (1990)
44. V. Foglietti, Double dc SQUID for flux-locked-loop operation. Appl. Phys. Lett. **59**, 476–478 (1991)
45. R.P. Welty, J.M. Martinis, Two-stage integrated SQUID amplifier with series array output. IEEE Trans. Appl. Supercond. **3**, 2605–2608 (1993)
46. M.E. Huber, P.A. Neil, R.G. Benson, D.A. Burns, A.F. Corey, C.S. Flynn, Y. Kitaygorodskaya, O. Massihzadeh, J.M. Martinis, G.C. Hilton, dc SQUID series array amplifiers with 120 MHz bandwidth. IEEE Trans. Appl. Supercond. **11**, 1251–1256 (2001)
47. J. Oppenländer, C. Häussler, N. Schopohl, Non Phi0 periodic macroscopic quantum interference in one-dimensional parallel Josephson junction arrays with unconventional grating structure. Phys. Rev. B. **63**, 024511 (2000)
48. C. Häussler, J. Oppenländer, N. Schopohl, Nonperiodic flux to voltage conversion of series arrays of dc superconducting quantum interference devices. J. Appl. Phys. **89**, 1875 (2001)
49. R. Cantor, F. Ludwig, in *SQUID Fabrication Technology*, ed by J. Clarke, A.I. Braginski. The SQUID Handbook vol. 1: Fundamentals and Technology of SQUIDs and SQUID systems (Wiley-VCH, Weinheim, 2004), pp. 93–126
50. H. Hayakawa, N. Yoshikawa, S. Yorozu, A. Fujimaki, Superconducting digital electronics. Proc. IEEE **92**, 1549–1563 (2004)
51. K.K. Likharev, Superconductor digital electronics. Physica C **482**, 6–18 (2012)
52. J.V. Gates, M.A. Washington, M. Gurvitch, Critical current uniformity and stability of Nb/Al–oxide–Nb Josephson junctions. J. Appl. Phys. **55**, 1419 (1984)
53. T. Lehnert, D. Billon, C. Grassl, K.H. Gundlach, Thermal annealing properties of Nb–Al/AlOx–Nb tunnel junctions. J. Appl. Phys. **72**, 3165 (1992)
54. S. Anders, M.G. Blamire, F.I. Buchholz, D.G. Crété, R. Cristiano, P. Febvre, L. Fritzsch, A. Herr, E. Il'ichev, J. Kohlmann, J. Kunert, H.G. Meyer, J. Niemeyer, T. Ortlepp, H. Rogalla, T. Schurig, M. Siegel, R. Stolz, E. Tarte, et al. European roadmap on superconductive electronics—status and perspectives. Physica C: Superconductivity. **470**, 2079–2126 (2010)
55. H.G. Meyer, L. Fritzsch, S. Anders, M. Schmelz, J. Kunert, G. Oelsner, in *LTS Josephson Junctions and Circuits*, ed by P. Seidel. Applied Superconductivity: Handbook on Devices and Applications (Wiley, Hoboken, 2015), pp. 281–297
56. H. Kroger, L.N. Smith, D.W. Jillie, Selective niobium anodization process for fabricating Josephson tunnel junctions. Appl. Phys. Lett. **39**, 280–282 (1981)
57. M. Gurvitch, M.A. Washington, H.A. Huggins, High quality refractory Josephson tunnel junctions utilizing thin aluminum layers. Appl. Phys. Lett. **42**, 472–474 (1983)
58. M. Maezawa, M. Aoyagi, H. Nakagawa, I. Kurosawa, S. Takada, Specific capacitance of $Nb/AlO_x/Nb$ Josephson junctions with critical current densities in the range of 0.1—18 kA/cm^2. Appl. Phys. Lett. **66**, 2134–2136 (1995)
59. S. Anders, M. Schmelz, L. Fritzsch, R. Stolz, V. Zakosarenko, T. Schönau, H.G. Meyer, Sub-micrometer-sized, cross-type Nb–AlOx–Nb tunnel junctions with low parasitic capacitance. Supercond. Sci. Technol. **22**, 064012 (2009)

60. M. Schmelz, R. Stolz, V. Zakosarenko, S. Anders, L. Fritzsch, M. Schubert, H.G. Meyer, SQUIDs based on submicrometer-sized Josephson tunnel junctions fabricated in a cross-type technology. Supercond. Sci. Technol. **24**, 015005 (2011)
61. M. Schmelz, R. Stolz, V. Zakosarenko, T. Schönau, S. Anders, L. Fritzsch, M. Mück, H.G. Meyer, Field-stable SQUID magnetometer with sub-fT $Hz^{-1/2}$ resolution based on sub-micrometer cross-type Josephson tunnel junctions. Supercond. Sci. Technol. **24**, 065009 (2011)
62. A. Chwala, J. Kingman, R. Stolz, M. Schmelz, V. Zakosarenko, S. Linzen, F. Bauer, M. Starkloff, M. Meyer, H.G. Meyer, Noise characterization of highly sensitive SQUID magnetometer systems in unshielded environments. Supercond. Sci. Technol. **26**, 035017 (2013)
63. J. Vrba, in *SQUID Gradiometers in Real Environment*, ed by H. Weinstock. Squid Sensors: Fundamentals, Fabrication, and Applications (Kluwer Academic Publishers, Dordrecht/Boston/London, 1996), pp. 117–178
64. K.P. Humphrey, T.J. Horton, M.N. Keene, Detection of mobile targets from a moving platform using an actively shielded, adaptively balanced SQUID gradiometer. IEEE Trans. Appl. Supercond. **15**, 753–756 (2005)
65. R. Stolz, *Supraleitende Quanten-interferenzdetektor-Gradiometer-Systeme für den geophysikalischen Einsatz* (University Jena, Jena, 2006)
66. B. Muhlfelder, W. Johnson, M.W. Cromar, Double transformer coupling to a very low noise SQUID. IEEE Trans. Magn. **19**, 303–307 (1983)
67. I.K. Harvey, A precise low temperature dc ratio transformer. Rev. Sci. Instrum. **43**, 1626–1629 (1972)
68. F. Gay, F. Piquemal, G. Geneves, Ultralow noise current amplifier based on a cryogenic current comparator. Rev. Sci. Instrum. **71**, 4592–4595 (2000)
69. C. Granata, A. Vettoliere, M. Russo, An ultralow noise current amplifier based on superconducting quantum interference device for high sensitivity applications. Rev. Sci. Instrum. **82**, 013901 (2011)
70. J. Luomahaara, M. Kiviranta, J. Hassel, A large winding-ratio planar transformer with an optimized geometry for SQUID ammeter. Supercond. Sci. Technol. **25**, 035006 (2012)
71. V. Zakosarenko, M. Schmelz, R. Stolz, T. Schönau, L. Fritzsch, S. Anders, H.G. Meyer, Femtoammeter on the base of SQUID with thin-film flux transformer. Supercond. Sci. Technol. **25**, 095014 (2012)
72. W. Wernsdorfer, in *Classical and Quantum Magnetization Reversal Studied in Nanometer-Sized Particles and Clusters*. Advances in Chemical Physics (Wiley, Hoboken, 2001), pp. 99–190
73. W. Wernsdorfer, Molecular magnets: a long-lasting phase. Nat. Mater. **6**, 174–176 (2007)
74. P. Bushev, D. Bothner, J. Nagel, M. Kemmler, K.B. Konovalenko, A. Lörincz, K. Ilin, M. Siegel, D. Koelle, R. Kleiner, F. Schmidt-Kaler, Trapped electron coupled to superconducting devices. Eu Phys. J. D. **63**, 9–16 (2011)
75. M. Schmelz, R. Stolz, V. Zakosarenko, S. Anders, L. Fritzsch, H. Roth, H.G. Meyer, Highly sensitive miniature SQUID magnetometer fabricated with cross-type Josephson tunnel junctions. Physica C **476**, 77–80 (2012)
76. K. Hasselbach, C. Veauvy, D. Mailly, MicroSQUID magnetometry and magnetic imaging. Physica C **332**, 140–147 (2000)
77. S.K.H. Lam, D.L. Tilbrook, Development of a niobium nanosuperconducting quantum interference device for the detection of small spin populations. Appl. Phys. Lett. **82**, 1078 (2003)
78. A.G.P. Troeman, H. Derking, B. Borger, J. Pleikies, D. Veldhuis, H. Hilgenkamp, NanoSQUIDs based on niobium constrictions. Nano Lett. **7**, 2152–2156 (2007)
79. L. Hao, J.C. Macfarlane, J.C. Gallop, D. Cox, J. Beyer, D. Drung, T. Schurig, Measurement and noise performance of nano-superconducting-quantum-interference devices fabricated by focused ion beam. Appl. Phys. Lett. **92**, 192507 (2008)

80. D. Vasyukov, Y. Anahory, L. Embon, D. Halbertal, J. Cuppens, L. Neeman, A. Finkler, Y. Segev, Y. Myasoedov, M.L. Rappaport, M.E. Huber, E. Zeldov, A scanning superconducting quantum interference device with single electron spin sensitivity. Nat Nano. **8**, 639–644 (2013)
81. J. Nagel, O.F. Kieler, T. Weimann, R. Wölbing, J. Kohlmann, A.B. Zorin, R. Kleiner, D. Koelle, M. Kemmler, Superconducting quantum interference devices with submicron Nb/HfTi/Nb junctions for investigation of small magnetic particles. Appl. Phys. Lett. **99**, 032506 (2011)
82. M. Schmelz, Y. Matsui, R. Stolz, V. Zakosarenko, T. Schönau, S. Anders, S. Linzen, H. Itozaki, H.G. Meyer, Investigation of all niobium nano-SQUIDs based on sub-micrometer cross-type Josephson junctions. Supercond. Sci. Technol. **28**, 015004 (2015)
83. D. Drung, Digital feedback loops for dc SQUIDs. Cryogenics **26**, 623–627 (1986)
84. H. Matz, D. Drung, E. Crocoll, R. Herwig, E. Kramer, M. Neuhaus, W. Jutzi, Integrated magnetometer with a digital output. Trans. Magn. IEEE **27**, 2979–2982 (1991)
85. N. Fujimaki, K. Gotoh, T. Imamura, S. Hasuo, Thermal-noise-limited performance in single-chip superconducting quantum interference devices. J. Appl. Phys. **71**, 6182 (1992)
86. T. Reich, P. Febvre, T. Ortlepp, F.H. Uhlmann, J. Kunert, R. Stolz, H.G. Meyer, Experimental study of a hybrid single flux quantum digital superconducting quantum interference device magnetometer. J. Appl. Phys. **104**, 024509 (2008)
87. T. Schönau, M. Schmelz, V. Zakosarenko, R. Stolz, M. Meyer, S. Anders, L. Fritzsch, H.G. Meyer, SQUID-based setup for the absolute measurement of the Earth's magnetic field. Supercond. Sci. Technol. **26**, 035013 (2013)